

CLASSIFICATION OF URBAN BLUE GREEN STRUCTURES WITH AERIAL MEASUREMENTS

THOMAS K. THIIIS¹, NIKI GAITANI², INGUNN BURUD¹ & JON ARNE ENGAN¹

¹Norwegian University of Life Sciences, Department of Mathematical Sciences and Technology
Campus Ås, Norway

²National and Kapodistrian University of Athens, Physics Department, Building Physics,
University Campus, Athens, Greece.

ABSTRACT

The development of climate-responsive design has social and environmental impacts, as the adverse effects of climate change are particularly relevant for urban areas. Green and blue infrastructure has been identified as best practice for achieving greater urban sustainability and resilience. The climatic improvements from use of blue-green infrastructure are generally related to the ability to moderate the impacts of extreme precipitation and temperature. However, the challenges and barriers to implementation of climate adaptation plans focusing on the use of blue-green spaces have not been analysed extensively to date.

The present work describes a novel methodology to measure and classify urban surface parameters, which are important for the understanding and simulation of urban flooding. An aerial survey with multispectral sensors in VIS/NIR (Visible and Near Infrared) and IR (Infrared) wavelengths on a UAV (Unmanned Airborne Vehicle) has been carried out at the campus of the Norwegian University of Life Sciences in Ås, Norway. The area covers various types of surface such as asphalt, concrete, gravel, vegetation and water. The Normalized Difference Vegetation Index (NDVI) derived from the VIS/NIR images have been used to study the spatial distribution and physical characteristics of the vegetation. Multivariate statistical tools have further been utilized to classify the different terrain materials according to their reflectance spectral properties from the multispectral VIS/NIR/IR data cubes. These materials have been linked to roughness and infiltration properties that are commonly used in water analysis simulation tools. Photogrammetry was applied to compute the Digital Surface Map (DSM), which was used to determine drainage lines and water accumulation areas in the surveyed area. The applied method provides data with high spatial resolution that can simplify and improve simulation of urban flooding.

Keywords: Materials, multispectral survey, unmanned airborne vehicle, vegetation, water permeability.

1 INTRODUCTION

Climate projections foresee a significant increase in the frequency and intensity of extreme events [1–3]. Especially on urban areas, climate change exerts additional stress through increased number of heat waves, more intense droughts and frequent inland floods and compromising water supplies [4–6].

One of the principle hazards in urban basins is the flooding due to the lack of drainage (namely urban pluvial flooding) [7]. The increased area of impervious surfaces in cities decreases the infiltration and increases the surface runoff, consequently increasing the risk of flooding [8]. Albeit the implementation of flood control infrastructure, modern cities remain vulnerable to the increased flood hazards [9].

Green and blue infrastructure has been identified as best practice for achieving greater urban sustainability and resilience. The blue-green components include all natural and semi-natural landscape elements as: lakes, retention ponds, swales and buffer strips, rain gardens, permeable surfaces, green alleys and streets, urban forestry, green open spaces such as parks and wetlands, and adapted buildings to better cope with floods and coastal storm surges [10].

The present study aims to measure with high-resolution aerial survey the different surface characteristics and classify the physical parameters, which are important for the understanding and the simulation of microscale flooding. The use of UAVs as a sensor platform is novel and provides flexibility in the timing of data captured and the scale of the images obtained.

2 MATERIALS AND DATA

The study has been carried out at the campus of the Norwegian University of Life Sciences in Ås, Norway. The area covers various types of surface such as asphalt, gravel, grass and water.

The applied multisensory survey included high-resolution recordings of the materials in the visible, near infrared (VIS/NIR) and infrared (IR) wavelength region. The flights were performed in a predetermined pattern at an altitude of 70 m. A total of approximately 200–300 partly overlapping images were recorded in each flight.

An RGB camera, a rebuild RGB camera where the blue channel is replaced by a NIR channel (Canon PowerShot rebuild by Maxmax.com) and an IR camera (FLIR Vue Pro 640, 9 mm lens) were used. The pixel size of the pictures varied from 8mm to 80 mm depending on the type of sensor. The IR photos were taken twice, before sunrise and at noon. This was in order to compute the Diurnal Temperature Amplitude (DTA), which was taken as the difference between maximum (noon) and minimum surface temperature (at dusk). Figure 2 shows the DTA and the NIR images of the area.



Figure 1: The study area (RGB photo taken from the UAV).

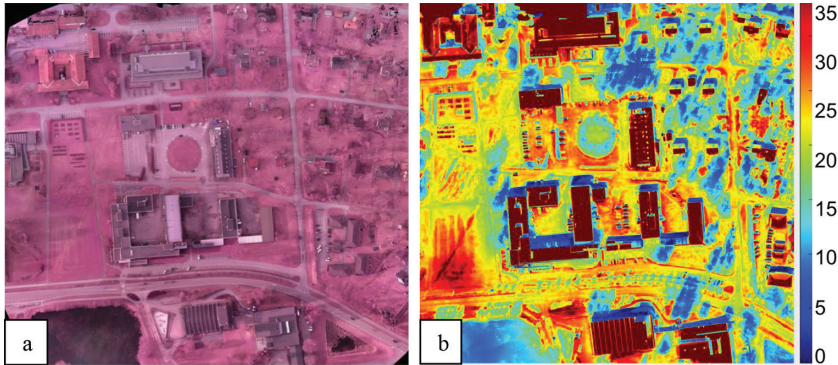


Figure 2: a) Near Infra-Red (NIR) image. b) Diurnal Temperature Amplitude (DTA) of the study area.

The images from the aerial surveys have been corrected for the geometric distortions (orthorectification process), and then transformed to geo-referenced raster images with the commercially available aerial image processing software Pix4D [11]. A digital surface model (DSM) is produced from photogrammetry of the RGB images in Pix4D. The ground sampling distance in the survey was 31 mm, which gives a resolution of the DSM and orthomosaic of 31 mm. The accuracy of the DSM produced is in the range of 31–93 mm. A standardized grey calibration plate reflecting 60% of the solar radiation was recorded before and after each set of VIS/NIR images. Close-up images of the different materials were also performed with all three cameras.

3 THEORY AND ANALYSIS

3.1 Analysis of flood paths and sinks

When intensive or long-lasting precipitation causes runoff in excess of the capacity of the urban drainage system, there is a potential for pluvial flooding. During urban pluvial flooding, pervious ground is typically saturated and therefore not capable of absorbing more water through infiltration. Surface storage provided by ponding, surface wetting, and interception will withhold some of the surface water and the excess water will stream and accumulate on the surface on its way to the receiver depending on the topography.

Flood flows are channelled across the landscape downstream in stream paths shaped by the topography and the built environment in the catchment and digital terrain models are routinely used to identify these paths and analyse the channel networks [12, 13]. The depth of the water as it streams and accumulates is influenced, amongst others, by the terrain gradient and the surface roughness. When the terrain gradient shifts from negative to positive, the water will pond until the water level again reaches a level with negative gradient. These ponds develop in natural or constructed depressions in the terrain called sinks. Water trapped in sinks will eventually disappear through infiltration, evapotranspiration, the drainage system or a combination of these.

Sinks, both in pervious and impervious areas, could be a positive element in reducing the effects of pluvial flooding as long as they are thoroughly mapped, regarding both depth and area, and connected to the drainage lines. Evapotranspiration is a slow-acting process so in sinks on pervious ground, there should be capacity for gradually infiltrating the water

and on impervious ground, the sinks should preferably be connected to the drainage network or SuDS (sustainable drainage system) so that the water can be diverted when capacity is available.

GIS analysis of digital terrain models are commonly used to identify sinks and flood paths and in this study ArcMap [14], which is the main component of Esri's ArcGIS suite of geospatial processing programs, is used with the Spatial Analyst extension to generate the area and depth of sinks and the paths of drainage lines illustrated in this paper. The basis for this process is a raster file with a high-resolution digital surface model (DSM) generated from the aerial photography.

The resolution of the DSM is much higher than what would be possible if the DSM was built from publicly available vector and LIDAR data and that is an important advantage when modelling the path of water on terrain were it is essentially details that govern which way the water will stream, absorb, detain and promote the infiltration of floodwater. For example can linear landscape features significantly affect the hydrological and geomorphological processes within a watershed and it has been shown that tillage furrows as small as 2 cm in depth can significantly modify flow networks and erosion patterns [15–19].

Various models are now available to analyse urban flooding, and these flood models are very valuable assets for an integrated water management in cities. Data availability is one of the main drivers for such a concept, and many factors can influence the choice of a flood modelling approach. Two-dimensional hydraulic surface models simulate surface flow with a level of accuracy depending mainly on topographical data resolution and model grid size of the DSM. These models also require the specification of flow resistance or 'roughness' parameters that can be specified individually for each computational cell [20] or to groups of cells that have the same characteristics. The simulated surface run-off (rainfall excess) in a hydraulic model is substantially influenced by the characterisation of infiltration in the model and can be classified to groups of computational cells in a similar way as with the roughness.

To manage pluvial flood risk, the capacity of the surfaces in water storage and water generation should be analysed in detailed maps. Comprehensive characteristics of the urban landscape surface are crucial to provide the best achievable input to model the important parameters on the water balance in the urban drainage basins, as surface roughness, permeability and evapotranspiration.

The velocity of a liquid flowing in an open channel can be estimated by the well-known Manning's formula. An important input to this formula is the surface roughness of the channel. The Manning's roughness coefficient (n) [21] is dependent on the surface material and values of the examined materials used in this study are given in Table 1.

Table 1: Manning's n values for the examined materials

Type of surface	Manning's n
Asphalt	0.013
Concrete pavement	0.014
Grass	0.03
Gravel	0.023

3.2 Classification of the terrain surfaces

The soil heterogeneity has an important role in the surface runoff. In order to classify the different surface characteristics according to their reflectance spectral properties, the ortho-photos in the four wavelength bands, Blue (B), Green (G), Red (R) and NIR, and the DTA from the difference IR images were resampled and aligned pixel to pixel and then stacked into one image cube. In addition, a map representing classes of materials derived from a texture analysis was included in the stack. The texture map of seven texture classes was derived using a Gray-Level Co-Occurrence Matrix (GLCM) algorithm in MATLAB [22]. The texture analysis is a technique to quantify the patterns in images by terms such as rough, smooth as function of the spatial variation in pixel intensities. Figure 3a shows the GLCM texture analysis of the orthophoto.

The soils and impervious surfaces have quite similar characteristics in certain wavelengths so it is challenging to identify and classify them. However, vegetation shows strong reflection in NIR and strong absorption in the red band. Water exhibits the high reflectance values at the blue (B) band and gradually decreases towards the NIR band [23]. With the aim of transforming the multispectral data into a single image which enhances the vegetation distribution, the Normalized Difference Vegetation Index (NDVI) was calculated. The NDVI algorithm subtracts the red reflectance values from the NIR and divides it by the sum of NIR and red bands according to the equation:

$$NDVI = (NIR - R) / (NIR + R) \quad (1)$$

where NIR and R are the reflectance values in the near infrared and red wavebands, respectively. The values of the index range from -1 to +1 and higher NDVI generally indicates more vegetation.

The DSM was also aligned with the stack of images. The DSM captures all the elevated surfaces, both natural and built features and was used to mask out buildings on the images in the stack in order to focus the analysis on the ground surface. When masking out all elevated areas according to a selected threshold, some trees will be misclassified as buildings. A second constraint in addition to the elevation threshold was therefore applied using the NDVI image. Given that vegetated areas have a value $NDVI > 0.5$, the masking of roofs was carried

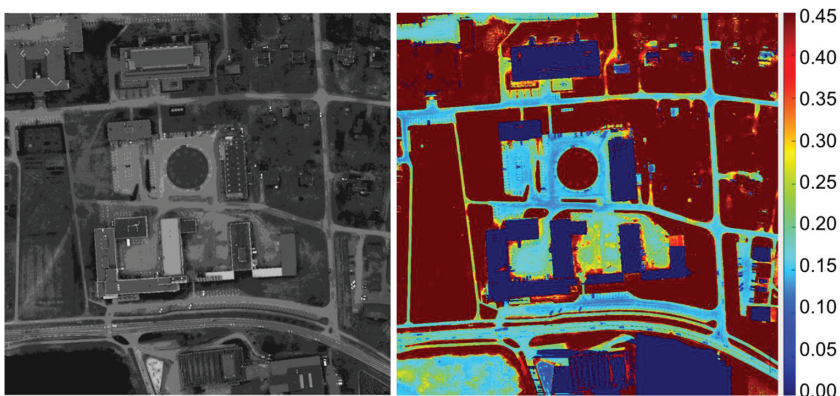


Figure 3 a) Left: GLCM texture analysis and b) Right: NDVI of the study area, roof tops masked as blue and vegetation as red.

out by selecting all pixels with both an elevation above the threshold value, and $NDVI < 0.5$. The pixels with $NDVI > 0.5$ were classified as vegetation and were therefore not masked as roof, even if they were elevated above the ground level.

The NDVI map of the study area is shown in Figure 3, where the roofs are masked and visualized with a dark blue colour. The cutoff in the display is set to 0.45 so that all vegetation appears with a solid red colour. Note that some of the red roofs and in particular the red roof with some algae growth on, in the upper left corner of the map (see Figure 1) are not masked as roofs. The reason for this is that their spectral reflectance yields a value of $NDVI > 0.5$, the same as for vegetation. The applied method for masking out roofs as described above, works only for roof materials with a different NDVI value than the vegetation.

To analyse the stack of six images (five spectral bands, B, G, R, NIR, IR and the texture map), a multivariate classification algorithm, and Partial least squares discriminant analysis (PLS-DA) was applied. PLS-DA is a supervised linear classification method, a derivative of the standard PLS regression that uses class variables instead of numeric variables. Classes of five different materials were selected manually from the images in the stack, vegetation, gravel, asphalt, water and roof. The roofs were already masked to a certain value using the DSM, and this was assigned to one of the classes. In order to validate the PLS-DA classification a separate image was constructed by manually selecting sections of the stack of maps with known materials and combines them into a mosaic. The regions selected were different from the ones used to construct the PLS-DA model.

The infiltration rate of rainwater into the soil is dependent on a number of different mechanisms. The infiltration of water starts at a constant rate f_0 and is decreasing exponentially with time. After some time when the soil saturation level reaches a certain value, the rate of infiltration will arrive at a constant rate f_c . This is dependent on the composition of the soil layer and the surface condition. Without knowledge of the subsurface structure of the soil, it is only possible to classify the infiltration properties into pervious and impervious surfaces. In this study, asphalt and concrete surfaces (mainly buildings, roads and parking spaces) are classified as impervious surfaces and the rest of the identified surfaces are classified as pervious to water. The infiltration rate in the pervious surfaces is dependent on already infiltrated water and subsurface soil structure.

4 RESULTS AND DISCUSSION

The aerial survey resulted in a number of maps that through classification analysis provide input on material properties needed for simulation of the blue-green structures.

An image of the texture analysis is shown in Figure 3. By comparing with the RGB image in Figure 1, it can be seen that water, vegetation, asphalt and gravel have different textures. However, in some areas, the classes are mixed, e.g. some worn areas on the grass and the asphalt have the same texture class as gravel.

On the DTA shown in Figure 2, it can be seen that the temperature variations are higher for the asphalt than for fresh vegetation. However, on the worn vegetation the soil is visible on the surface which has a larger temperature difference. The trees and shadow from the trees clearly show up as areas with small temperature changes between day and night.

The result from the supervised PLS-DA classification is shown in Figure 4. The classes for water, asphalt/concrete, gravel/stone, vegetation and roofs are indicated. The classes for asphalt/concrete, vegetation and gravel can be directly linked to the Manning's coefficient values in Table 1. Note that, as for the texture analysis, the asphalt and gravel areas are misclassified in some areas, mainly due to the inhomogeneity in the asphalt areas from tire tracks, cracks etc.

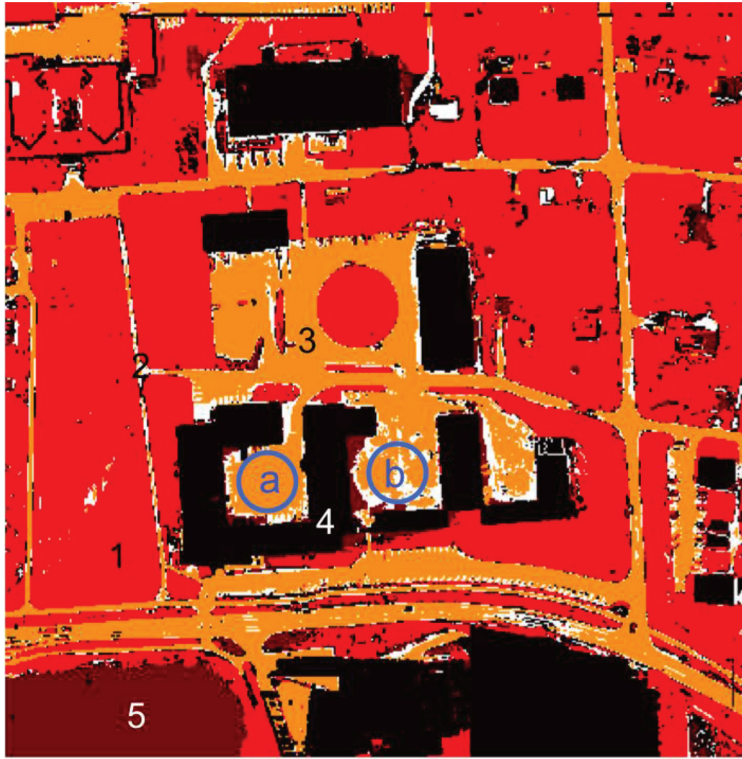


Figure 4: PLS-DA classification. The marked classes correspond to: 1) vegetation, 2) gravel/stone, 3) asphalt/concrete, 4) roofs and 5) water. The two blue circles indicate the close-up areas shown in Figure 5.

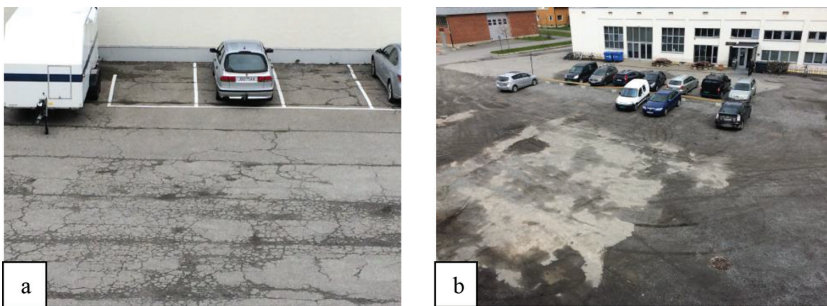


Figure 5: a) cracks in the asphalt. b) Mix of asphalt and gravel in the courtyard. Areas are indicated in Fig. 4.

Some parts of the asphalt have very similar reflectance properties as gravel, such as the close-ups from the backyard of one of the buildings, shown in Figure 5. The photos in Figure 5 display an asphalted area with many cracks and an area with a mixture of both asphalt and gravel. These two areas are marked with circles on the classification map in Figure 4. Note that the classification in these areas also yields a mixture of gravel and asphalt, consistent with the close ups in Figure 5.

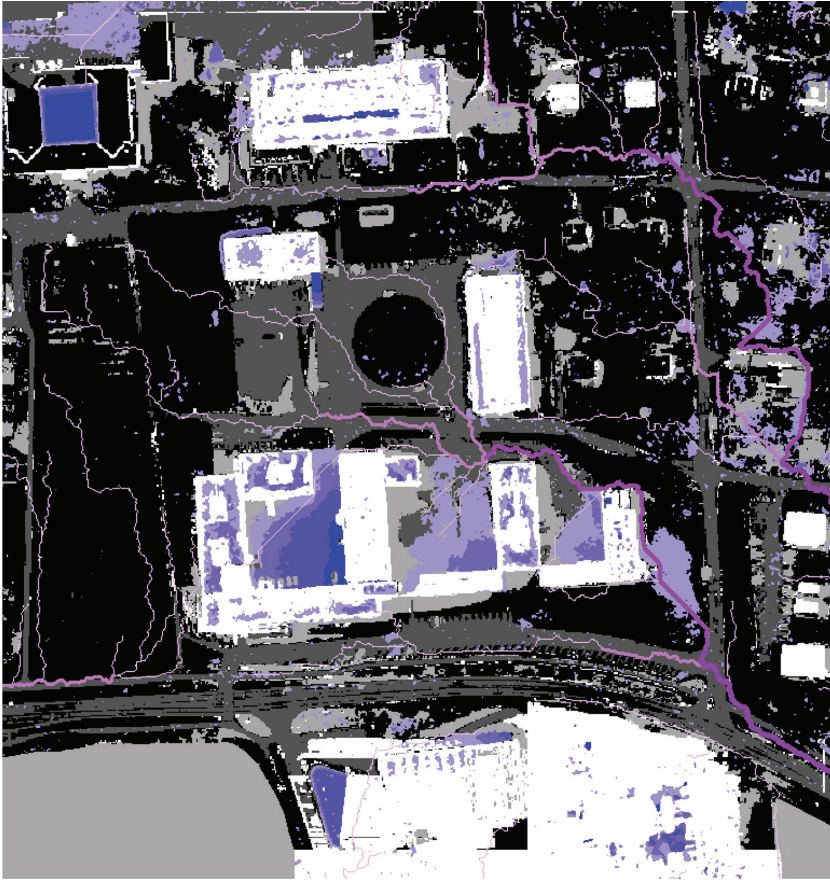


Figure 6: Drainage lines, sinks and water accumulation areas shown on a background that identifies the ground in the study area as either pervious (black) or impervious (dark gray).

The classification in Figure 4 can also be used to group the materials into pervious (vegetation, stone and gravel) and impervious surfaces (asphalt, concrete), which is linked to the analysis of sinks and drainage lines in the study area as shown in Figure 6. The figure visualizes the extent and depth of sinks and the path of the drainage lines in case of urban pluvial flooding.

Figure 6 shows the extent and depth of sinks and the path of the drainage lines in case of urban pluvial flooding in the study area. The purple drainage lines are classified according to the upstream catchment area of each point on the line and the classification was visualized with the width of the line. In a similar way, the sinks can be visualized according to their depth, and in Figure 6, the darkest blue color indicates the deepest areas. The drainage lines and sinks are shown on a background that identifies the ground in the study area as either pervious (black) or impervious (dark gray) as described earlier. Buildings and water, including wetted ground, are also identified (white and light gray).

The applied methodology identifies the flow paths and areas prone to accumulation of water in the current terrain or built environment but the methodology could also be used as a planning tool were proposals for new development can be tested for its resilience to

urban flooding as long as a 3D terrain model can be established. In feasibility studies, new development, infrastructure or solutions can be included in the 3D terrain model and modified or changed until water flows and accumulate were it does no harm.

The high resolution of the 3D terrain model established is important in GIS modeling of drainage lines. The classification of surface properties such as roughness and infiltration provided in this study can further be used in a 2D hydraulic simulation. The flexibility of the present methodology makes it a well-suited tool to specify important parameters and to integrate them in simulations to fully take advantage of the hydraulic model.

5 CONCLUDING REMARKS

Urban flooding reduction and prevention can be achieved by implementing sustainable urban drainage with the three-stage principles of infiltration, retention and securing safe flood paths in the urban design process. Despite complex setup and lack of surface property maps, modelling urban flooding is becoming a practical tool in urban planning.

This paper shows that input to urban flood simulation can be largely simplified with the use of UAV, optical sensors and automated classification. This study shows that photogrammetry can produce DSMs with an accuracy adequate for flow accumulation simulations. In addition, analysis of thermal and optical properties of the surface can classify pervious and impervious surfaces as well as give spatial information of the surface roughness of the urban fabric.

REFERENCES

- [1] EPRS. Developing an EU urban agenda, 2015.
- [2] United Nations, *World Urbanization Prospects: The 2014 Revision*. United Nations, NY, 2014.
- [3] Urban Climate Change Research Network UCCRN. (2011) *Climate Change and Cities First Assessment Report*
- [4] The New Urban Agenda, Habitat III, 2016.
- [5] Solomon, S., Qin, D., Manning, M., Chen, Z., Marquis, M., Averyt, K.B., Tignor, M. & Miller, H.L., (eds.). Climate change, the physical science basis. In: *Contribution of the Working Group I to the Fourth Assessment Report of the Intergovernmental Panel on Climate Change*, Cambridge University Press, Cambridge, pp. 996, 2007.
- [6] Intergovernmental Panel on Climate Change IPCC. *Climate Change 2014: Synthesis Report*, IPCC, Geneva, Switzerland, 2014.
- [7] Priest, S.J., Parker, D.J., Hurford, A.P., Walker, J. & Evans, K., Assessing options for the development of surface water flood warning in England and Wales. *Journal of Environmental Management*, **92**(12), pp. 3038–3048, 2011.
<https://doi.org/10.1016/j.jenvman.2011.06.041>
- [8] Jha, A.K., Bloch, R. & Lamond, J., *Cities and Flooding. A Guide to Integrated Urban Flood Risk Management for the 21st Century*. The World Bank, Washington DC, 2012.
- [9] Liao, K-H. & Chan, J.K.H., Urban design principles for flood resilience: learning from the ecological wisdom of living with floods in the Vietnamese Mekong Delta. *Land-scape and Urban Planning*, **155**, pp. 69–78, 2016.
<https://doi.org/10.1016/j.landurbplan.2016.01.014>
- [10] Demuzere, M., Orru, K., Heidrich, O., Olazabal, E., Geneletti, D., Orru, H., Bhawe, A.G., Mittal, N., Feliu, E. & Faehnle, M., Mitigating and adapting to climate change: multi-functional and multi-scale assessment of green urban infrastructure. *Journal of Environmental Management*, **146**, pp. 107–115, 2014.
<https://doi.org/10.1016/j.jenvman.2014.07.025>

- [11] PIX4d Software: Available at: <https://pix4d.com/>. (Accessed 15 May 2017).
- [12] Moore, I.D., Grayson, R.B. & Ladson, A.R., Digital terrain modelling: a review of hydrological geomorphological and biological applications. *Hydrological Processes*, **5**, pp. 3–30, 1991.
<https://doi.org/10.1002/hyp.3360050103>
- [13] Tarboton, D.G., Bras, R.L. & Rodriguez-Iturbe, I., On the extraction of channel networks from digital elevation data. *Hydrological Processes*, **5**, pp. 81–100, 1991.
<https://doi.org/10.1002/hyp.3360050107>
- [14] ARC GIS: Available at: <http://desktop.arcgis.com/en/arcmap/>. (Accessed 15 May 2017).
- [15] Ludwig, B., Daroussin, J., King, D. & Souchere, V., *Using GIS to predict concentrated flow erosion in cultivated catchments*. Proceedings of the HydroGIS 96: Applications of Geographic Information Systems in Hydrology and Water Resources Management held in Vienna, Austria, 1996.
- [16] Snaddon, C.D., Wishart, M.J. & Davies, B.R., Some implications of inter-basin water transfers for river ecosystem functioning and water resources management in southern Africa. *Aquatic Health and Management*, **1**, pp. 159–182, 1998.
<https://doi.org/10.1080/14634989808656912>
- [17] Cerdan, O., Souchere, V., Lecomte, V., Couturier, A. & Le Bissonnais, Y., Incorporating soil surface crusting processes in an expert-based runoff model: sealing and transfer by runoff and erosion related to agricultural management. *Catena*, **46**, pp. 189–205, 2001.
[https://doi.org/10.1016/s0341-8162\(01\)00166-7](https://doi.org/10.1016/s0341-8162(01)00166-7)
- [18] Tak ken, I., Govers, G., Steegen, A., Nachtergaele, J. & Guerif, J., The prediction of runoff flow directions of tilled fields. *Journal of Hydrology*, **248**, pp. 1–13, 2001.
[https://doi.org/10.1016/s0022-1694\(01\)00360-2](https://doi.org/10.1016/s0022-1694(01)00360-2)
- [19] Souchere, V., Cerdan, O., Ludwig, B., Le Bissonnais, Y., Couturier, A. & Papy, F., Modelling ephemeral gully erosion in small cultivated catchments. *Catena*, **50**, pp. 489–505, 2003.
[https://doi.org/10.1016/s0341-8162\(02\)00124-8](https://doi.org/10.1016/s0341-8162(02)00124-8)
- [20] Hunter, N., Bates, P., Horritt, M. & Wilson, M., Simple spatially-distributed models for predicting flood inundation: a review. *Geomorphology*, **90**, pp. 208–225, 2007.
<https://doi.org/10.1016/j.geomorph.2006.10.021>
- [21] Manning's n values for Channels, Closed Conduits Flowing Partially Full, and Corrugated Metal Pipes: Available at: http://www.fsl.orst.edu/geowater/FX3/help/8_Hydraulic_Reference/Mannings_n_Tables.htm. (Accessed 15 May 2017).
- [22] MATLAB, GLCM algorithm: Available at: <https://se.mathworks.com/help/images/gray-level-co-occurrence-matrix-g lcm.html?requestedDomain=www.mathworks.com/>. (Accessed 15 May 2017).
- [23] Colaninno, N., Roca, J., Burns, M. & Alhaddad, B., Defining densities for urban residential texture through land use classification, from LANDSAT TM imagery: Case study of Spanish Mediterranean coast. International Archives of the Photogrammetry, Remote Sensing and Spatial Information Sciences, Volume XXXIX-B7, XXII ISPRS Congress, Melbourne, Australia, 2012.